Letter

Ultrasonic Extraction and Manipulation of Droplets from a Liquid-Liquid Interface with Near-Field Acoustic Tweezers

Robert Lirette,[*] Joel Mobley,[†] and Likun Zhang[‡]
Department of Physics and Astronomy and the National Center for Physical Acoustics, The University of Mississippi, University, Mississippi 38677, USA

(Received 7 September 2019; revised manuscript received 13 November 2019; published 16 December 2019)

We report the extraction, capture, and manipulation of a droplet from a liquid-liquid surface using the acoustic near field from a fraxicon lens transducer. The lens is submerged in water, which shares a planar boundary with a reservoir of carbon tetrachloride (CCl_4). The ultrasonic beam exerts a negative radiation pressure, drawing the CCl_4 up into the water, and a droplet of wavelength order is extracted out of the bulk liquid and sonically trapped. Our work demonstrates the means of producing and manipulating droplets from a fluid interface without mechanical contact using a near-field acoustic tweezer.

DOI: 10.1103/PhysRevApplied.12.061001

I. INTRODUCTION

The acoustic radiation force and associated trapping by acoustic tweezers has proven to be an efficient means of particle-manipulation applications [1–4]. Here we report on a near-field acoustic tweezer for droplet extraction and manipulation from a fluid-fluid interface. The ability to controllably extract liquid droplets of uniform size from a fluid interface with ultrasonic fields has not been previously reported and can be of great importance in laboratory and industry.

The effect of acoustic or optical fields on fluid interfaces has been demonstrated in prior works [5–8]. In 1939, negative radiation pressure was first demonstrated [5], and it depends on the energy density of the incident sound [9]. In prior studies, ultrasound beams with sufficient focus and intensity were used to deform the fluid interface [10], or eject droplets from the interface [11], although without controlled extraction and trapping.

Various objects have been trapped and manipulated using acoustic fields [12–19]. Typically a standing-wave field or that from a transducer array is required for trapping, although highly focused single-beam transducers have been used as well. Metasurface-based passive phased arrays or three-dimensional printed lenses have also been employed for particle manipulation [20–24]. In each of these cases, the trapping is highly sensitive to the object and beam parameters. Here, a near-field structure is responsible for the extraction, trapping, and manipulation of the droplet, effectively forming a potential well from the pressure gradient that automatically traps the droplet of wavelength order after the extraction.

The extraction and capture is achieved with the near field produced by a fraxicon acoustic lens. The fraxicon is a stepped lens containing no curved surfaces. It is designed to alter the phase of an ultrasonic field in discrete steps so that constructive interference occurs along a line through an extended depth of focus (DOF). The fraxicon is quasi-planar and is designed to mimic an axicon, which is a bulk refractive lens that produces a Bessel beam in the far field [25–27]. However, it is the *near-field* structure of the fraxicon that contains the pressure gradients responsible for the processes reported here.

II. METHODS

The setup consists of an ultrasonic transducer with the attached lens (referred to as the fraxicon transducer) immersed in a water bath above a reservoir of CCl_4 as shown in Fig. 1(a). The fraxicon transducer sits in 1 l of distilled water. Since CCl_4 has a higher density it supports the water layer. CCl_4 is immiscible with water and a planar boundary forms between the two. The acoustic impedances of water and CCl_4 are very nearly matched, which minimizes reflection from the interface. The transducer is driven by a rf generator and the electrical power delivered is monitored with a power meter. The transducer is operated at 1.20 MHz and registered no reflected rf power. All observations are recorded using either an Edgertronic high-speed video camera or a Canon EOS Rebel camera.

The fraxicon is designed to create constructive interference along its DOF. The surface of the lens is machined into a series of concentric rings of uniform thickness and discrete heights, shown in Fig. 1(b), which provide the

[*]rlirette@go.olemiss.edu
[†]jmobley@olemiss.edu
[‡]zhang@olemiss.edu

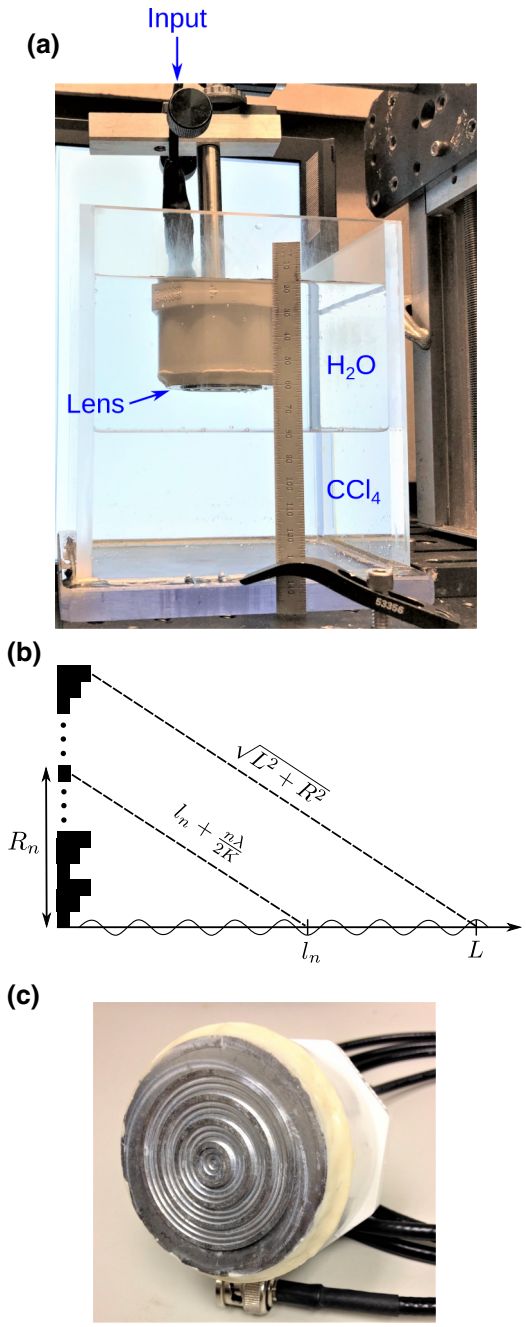

FIG. 1. (a) Experimental setup for insonifying the interface between water and CCl_4. The transducer is located in water and the propagation direction is downward into the CCl_4. (b) Radial profile of the fraxicon phase plate lens. (c) The assembled transducer with the fraxicon lens.

necessary phase shifts (see details in Sec. I of the Supplemental Material [28]). The fraxicon lens used in this work is made of aluminum and machined to shape. Aluminum is used as a lens material since it has low attenuation and will not deform from heating with higher source powers. The lens is directly bounded to a 50-mm PZT wafer with 3M DP270 epoxy. Figure 1(c) shows the transducer

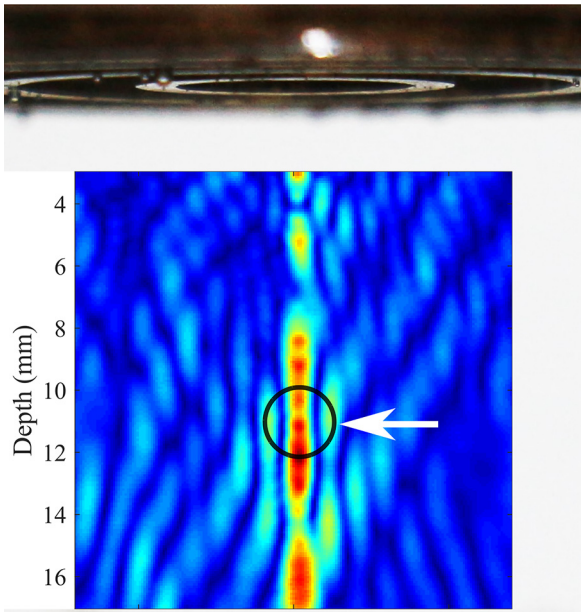

FIG. 2. Near-field axial plane data from hydrophone-scan measurements. The color scale represents the normalized amplitude of the 1.2 MHz spectral component of the field data. The depth is measured from the front of the lens. The scan width is 14 mm. The lens is shown at the top for scale.

after assembly. The PZT wafer has a wrap-around contact enabling it to be flush mounted to the lens. The transducer is enclosed in a PVC housing and water sealed with marine epoxy. In order to map the near field of the beam, the pressure field generated by the fraxicon transducer is measured over a two-dimensional grid using a computer-controlled hydrophone-scanning system (see details in Sec. II of the Supplemental Material [28]). The results are shown in Fig. 2 and the near-field trapping zone is identified.

III. RESULTS

The top row of Fig. 3(a) depicts negative radiation pressure exerted on the CCl_4 boundary, which draws a column of fluid into the water. When the source is placed between 12 and 18 mm from the boundary, the CCl_4 surface is pulled into the near-field region of the beam and around 11.8 mm from the lens, a droplet is extracted about 600 ms after irradiation begins. The extraction and trapping process is shown in a series of images in the bottom row of Fig. 3(a). A video is provided in the Supplemental Material ([[28], Video 1]). Note that the effective weight of the droplet is in the direction opposite to the extraction. The experiment was repeated for acoustic powers from 7 to 19 W, and all produced the same size droplet at the same distance from the lens. The time to form the droplet decreased with higher-power levels. For droplet extraction to occur the lens needs to be located within 19 mm of the interface while the droplet is always extracted 11.8 mm from the lens.

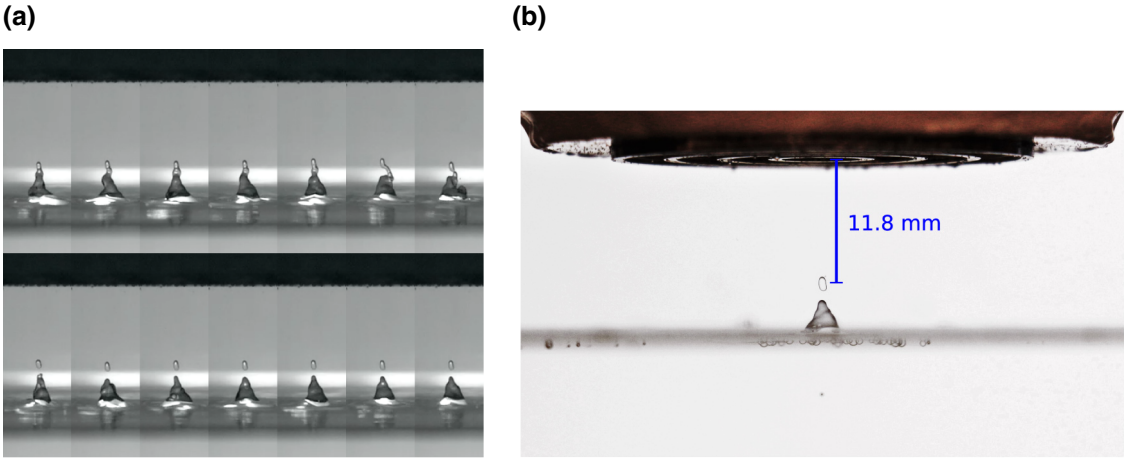

FIG. 3. (a) Images of the extraction process captured from high-speed video. Each frame is spaced 20 ms apart running from top left to bottom right. The first frame is taken 434 ms after the transducer power is turned on. The droplet extraction occurs between the seventh and eighth frames approximately 600 ms after power is applied. (b) Droplet trapped by the field from the fraxicon at a distance of 11.8 mm.

As shown in Fig. 3(a) when the fluid column is drawn upward, it thins and grows more chaotic, and a spheroidal droplet approximately 1.5 mm in height and 0.4 mm in width is extracted. The droplet stays trapped in the near-field pocket as seen in Fig. 3(b). The acoustic field in this region traps the droplet firmly, and it then can be manipulated vertically, laterally, and angularly by translating and rotating the source as seen in Fig. 4 and in the Supplemental Material ([[28], Videos 2 and 3]). The extraction-trapping process also works with the source at an angle to the surface. This indicates that a standing-wave condition is not required with this method.

Numerical calculations were performed to determine the radiation forces exerted on the droplet using the finite-element method (FEM) in the COMSOL environment (see details in Sec. III of the Supplemental Material [28]). In these calculations, a spheroidal droplet is placed at various depths along the axis of the source consisting of a uniform circular field passed through a fraxicon lens. At each depth the fields and forces are calculated. The Gor'kov potential for a small object in the long-wavelengh regime [26] cannot be used here as the droplet size (around 1.5 mm) is near the wavelength (1.23 mm), and multipolar scattering from the droplet is a significant factor. The vertical component of the force is calculated by integrating the radiation stress tensor of the incident and scattered fields over a cylindrical surface surrounding the region containing the droplet. Using the simulated incident and scattered fields, the vertical component of the force is calculated at each depth using [27,29]

$$\mathbf{F} = \int_S \left(\frac{\rho}{2} \langle |\mathbf{u}|^2 \rangle - \frac{1}{2\rho c^2} \langle p^2 \rangle \right) d\mathbf{A} - \int_S \rho \langle \mathbf{uu} \rangle \cdot d\mathbf{A}, \quad (1)$$

where $\mathbf{u}$ is the fluid-particle velocity, p is the acoustic pressure, and S is a cylindrical surface enclosing the droplet. The surface height and radius are chosen to be three times the droplet dimensions.

The results are shown in Fig. 5. The calculations predict a negative (upward) force suitable for trapping the droplet at around 11 mm from the lens, which is consistent with the experimentally observed depth. At that location, the negative radiation force exceeds the effective weight (2.74 μN) of the spheroidal droplet. The upward force required to balance this is represented by the dashed line in Fig. 5.

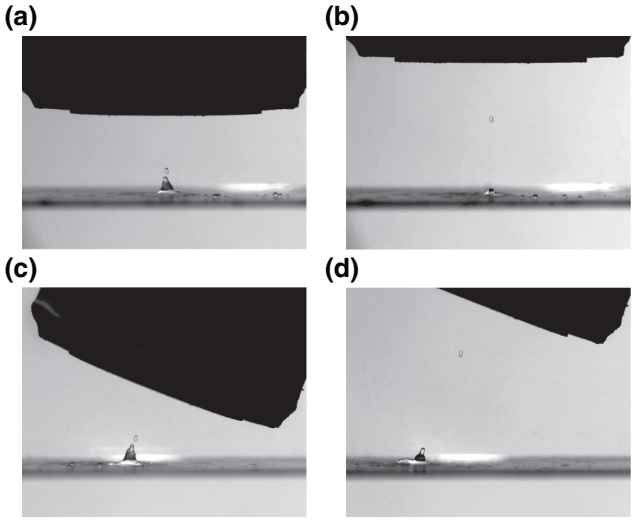

FIG. 4. Droplet capture and transport by the fraxicon transducer. The source power is 7.2 W. The fraxicon lens is (a) 16 mm from the fluid boundary and (b) transported upwards by 12 mm. Set at an angle with respect to the fluid boundary, the lens is (c) 18 mm from the fluid boundary and then (d) translated upwards by 19 mm.

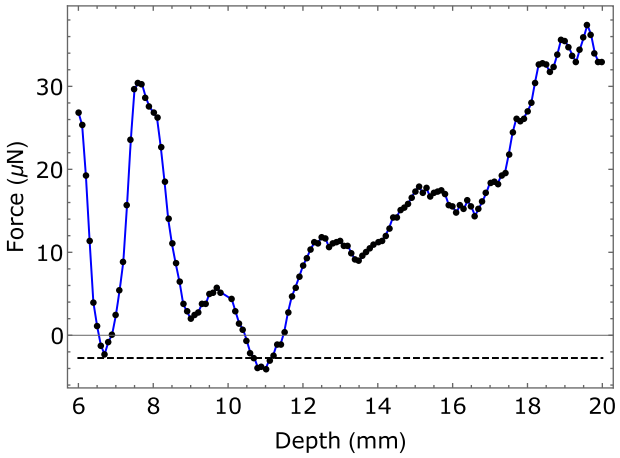

FIG. 5. Numerical result for the vertical component of the radiation force experienced by the CCl_4 droplet in water, taken from the FEM simulations. The depth is with respect to the front of the lens. The dashed line at the bottom represents the force required to balance the effective weight of the droplet.

IV. DISCUSSION

The controlled acoustic droplet extraction with subsequent capture from a fluid boundary has not been previously reported and is accomplished using near-field acoustic tweezers. With the near field of the fraxicon transducer insonifying a water-CCl_4 interface with an acoustic power of around 8 W, the radiation pressure is strong enough to pull the boundary layer into the near-field zone, which is capable of extracting a single droplet. In the beam pocket, the trapping forces are strong enough that the extracted droplet of wavelength order could then be transported throughout the water bath. This demonstrates the trapping phenomenon did not require standing-wave conditions since it is sustained when the transducer is moved away from the boundary via translation and/or rotation. The consistency of the numerical simulations of the force curve with the experimental results are also indicative that this is a free-field phenomenon.

Unlike a conventional Fresnel lens with curved surface features, the fraxicon is a stepped lens with a surface devoid of curvature. The thickness of the lens is less than the wavelength in aluminum and is straightforward to construct. It is meant to approximate the field from an axicon, which is a bulk-type conical lens that produces a Bessel beam in the far field. In previous work, characterizing the two lenses, the near field extended out to 25 mm from the source [30]. The extraction is performed well within the near field of the beam. The map of the near-field pressure amplitude of its near field shown in Fig. 2 shows the pocket structure responsible for the extraction process. In the vertical direction on the axis on both ends of this structure are pressure maxima. In the lateral direction is a cylindrical wall formed of a pressure maximum. This creates an acoustic potential well, which is responsible for the controlled extraction and trapping phenomena.

The radiation pressure based on a collimated planar beam incident on a liquid-liquid boundary is given by the relation [31]

$$P_{\text{net}} = E_I\left[1 - \frac{c_1}{c_2} + r_{12}^2\left(1 + \frac{c_1}{c_2}\right)\right], \tag{2}$$

$$r_{12} = \frac{\rho_2 c_2 - \rho_1 c_1}{\rho_2 c_2 + \rho_1 c_1}, \tag{3}$$

where E_I is the incident energy density, c_1 and ρ_1 are the speed of sound and density in the source fluid, c_2 and ρ_2 are the speed of sound and density in the target fluid, and r_{12} is the reflection coefficient. Equation (2) is applicable to a beam whose transverse profile is sufficiently smooth. The sign of the radiation pressure depends on the relative densities and sound speeds of the fluids (see illustration in Sec. IV of the Supplemental Material [28]). Once the surface is deformed, the radiation pressure on the curved plane can be calculated from the acoustic radiation pressure associated with the field or estimated from the balance with the gravito-capillary pressure. The water to CCl_4 interface experiences a negative radiation pressure while the sign would be reversed in a CCl_4 to water configuration. Note that in both cases, the boundary is deformed into the water. However, in subsequent work with other liquids we have found that extraction is possible in the opposite direction to the radiation pressure.

The ability to extract an intact sample of a liquid from a reservoir without mechanical contact can be of great utility in a variety of laboratory and industrial settings. That this is accomplished using a single source modified by a planar lens allows for the implementation of this method into laboratory environments without the need for a complex setup. Furthermore, the process could be scaled to extract and manipulate larger droplets, widening its applicability. Future work will concentrate on optimizing the field geometry and pressure gradients required for extraction. Thus this type of near-field acoustic tweezer could enable the effect to occur at lower powers and for different liquid combinations.

[1] Likun Zhang, From acoustic radiation pressure to three-dimensional acoustic radiation forces, J. Acoust. Soc. Am. **144**, 443 (2018).

[2] Long Meng, Feiyan Cai, Fei Li, Wei Zhou, Lili Niu, and Hairong Zheng, Acoustic tweezers, J. Phys. D: Appl. Phys. **52**, 273001 (2019).

[3] Mengxi Wu, Adem Ozcelik, Joseph Rufo, Zeyu Wang, Rui Fang, and Tony Jun Huang, Acoustofluidic separation of cells and particles, Microsyst. Nanoeng. **5**, 32 (2019).

[4] M. Baudoin and J.-L. Thomas, Acoustic tweezers for particle and fluid micromanipulation, Annu. Rev. Fluid Mech. **52**, 205 (2020).

[5] G. Hertz and H. Mende, Der schallstrahlungsdruck in flüssigkeiten, *Zeitschrift für Physik* (now Owned by Springer) 114, 354 (1939).

[6] B. Issenmann, A. Nicolas, R. Wunenburger, S. Manneville, and J.-P. Delville, Deformation of acoustically transparent fluid interfaces by the acoustic radiation pressure, EPL (Europhys. Lett.) **83**, 34002 (2008).

[7] Ming K. Tan, James R. Friend, and Leslie Y. Yeo, Interfacial Jetting Phenomena Induced by Focused Surface Vibrations, Phys. Rev. Lett. **103**, 024501 (2009).

[8] N. Bertin, H. Chraïbi, R. Wunenburger, J.-P. Delville, and E. Brasselet, Universal Morphologies of Fluid Interfaces Deformed by the Radiation Pressure of Acoustic or Electromagnetic Waves, Phys. Rev. Lett. **109**, 244304 (2012).

[9] R. T. Beyer, *Nonlinear Acoustics* (Naval Ship Systems Command, Department of the Navy, Washington, DC, 1976), Chap. VI, p. 221.

[10] L. Ostrovsky, S. Tsyuryupa, and A. Sarvazyan, Microsecond-range dynamics of tissues under the action of acoustic radiation force, Acta Acust. United Acust. **104**, 259 (2018).

[11] A. P. Brysev, F. Zoueshtiagh, P. Pernod, V. L. Preobrazhensky, and D. Makalkin, Droplet ejection from an interface between two immiscible liquids under pulsed ultrasound, Phys. Wave Phenom. **24**, 238 (2016).

[12] Lawrence A. Crum, Acoustic force on a liquid droplet in an acoustic stationary wave, J. Acoust. Soc. Am. **50**, 157 (1971).

[13] Junru Wu, Acoustical tweezers, J. Acoust. Soc. Am. **89**, 2140 (1991).

[14] Philip L. Marston and David B. Thiessen, Manipulation of fluid objects with acoustic radiation pressure, Ann. N. Y. Acad. Sci. **1027**, 414 (2004).

[15] Jungwoo Lee, Shia-Yen Teh, Abraham Lee, Hyung Ham Kim, Changyang Lee, and K. Kirk Shung, Single beam acoustic trapping, Appl. Phys. Lett. **95**, 073701 (2009).

[16] Youngki Choe, Jonathan W. Kim, K. Kirk Shung, and Eun Sok Kim, Microparticle trapping in an ultrasonic bessel beam, Appl. Phys. Lett. **99**, 233704 (2011).

[17] Asier Marzo, Sue Ann Seah, Bruce W. Drinkwater, Deepak Ranjan Sahoo, Benjamin Long, and Sriram Subramanian, Holographic acoustic elements for manipulation of levitated objects, Nat. Commun. **6**, 8661 (2015).

[18] Diego Baresch, Jean-Louis Thomas, and Régis Marchiano, Observation of a Single-Beam Gradient Force Acoustical Trap for Elastic Particles: Acoustical Tweezers, Phys. Rev. Lett. **116**, 024301 (2016).

[19] Michaël Baudoin, Jean-Claude Gerbedoen, Antoine Riaud, Olivier Bou Matar, Nikolay Smagin, and Jean-Louis Thomas, Folding a focalized acoustical vortex on a flat holographic transducer: Miniaturized selective acoustical tweezers, Sci. Adv. **5**, eaav1967 (2019).

[20] Yong Li, Xue Jiang, Bin Liang, Jian-Chun Cheng, and Likun Zhang, Metascreen-Based Acoustic Passive Phased Array, Phys. Rev. Appl. **4**, 024003 (2015).

[21] Kai Melde, Andrew G. Mark, Tian Qiu, and Peer Fischer, Holograms for acoustics, Nature **537**, 518 (2016).

[22] Gianluca Memoli, Mihai Caleap, Michihiro Asakawa, Deepak R. Sahoo, Bruce W. Drinkwater, and Sriram Subramanian, Metamaterial bricks and quantization of meta-surfaces, Nat. Commun. **8**, 14608 (2017).

[23] A. Franklin, A. Marzo, R. Malkin, and B. W. Drinkwater, Three-dimensional ultrasonic trapping of micro-particles in water with a simple and compact two-element transducer, Appl. Phys. Lett. **111**, 094101 (2017).

[24] A. Marzo, A. Ghobrial, L. Cox, M. Caleap, A. Croxford, and B. W. Drinkwater, Realization of compact tractor beams using acoustic delay-lines, Appl. Phys. Lett. **110**, 014102 (2017).

[25] Ilya Golub, Fresnel axicon, Opt. Lett. **31**, 1890 (2006).

[26] Xu-Dong Fan and Likun Zhang, Trapping Force of Acoustical Bessel Beams on a Sphere and Stable Tractor Beams, Phys. Rev. Appl. **11**, 014055 (2019).

[27] Likun Zhang and Philip L. Marston, Geometrical interpretation of negative radiation forces of acoustical Bessel beams on spheres, Phys. Rev. E **84**, 035601 (2011).

[28] See Supplemental Material at http://link.aps.org/supplemental/10.1103/PhysRevApplied.12.061001 for details of fraxicon lens design, hydrophone-scanning system, finite-element simulations, and three videos taken in experiments.

[29] Peter J. Westervelt, The theory of steady forces caused by sound waves, J. Acoust. Soc. Am. **23**, 312 (1951).

[30] R. Lirette and J. Mobley, Broadband wave packet dynamics of minimally diffractive ultrasonic fields from axicon and stepped fraxicon lenses, J. Acoust. Soc. Am. **146**, 103 (2019).

[31] T. G. Wang and C. P. Lee, in *Nonlinear Acoustics*, edited by M. F. Hamilton and D. T. Blackstock (Academic Press, San Diego, CA, 1998), Chap. 6, p. 187.